Visualization of in-vitro Blood Vessels in Contrast Images Based on Discrete Wavelet Transform Decomposition

F. Lopez-Tiro[1], H. Peregrina-Barreto[2], J. Rangel-Magdaleno[3], J. C. Ramirez-San-Juan[4]
[1]Biomedical Science and Technology Department, [2]Computer Science Department,
[3]Electronics Department, [4]Optics Department
Instituto Nacional de Astrofisica, Optica y Electronica
Luis Enrique Erro 1, Santa Maria Tonantzintla, 72840. Puebla, Mexico
Corresponding author: hperegrina@inaoep.mx

***Abstract*— Visualization of blood vessels in contrast images is an important task as it is used to analyze the dynamics of the blood flow and the health status of biological tissue. However, this task becomes difficult due to the noise in the image, mainly at high depths. This work proposes a methodology based on the Discrete Wavelet Transform to improve in-vitro blood vessels visualization. It also addresses the segmentation of the regions of interest through morphological operations in improved contrast images. Results show that it is possible to visualize the blood vessels even at 700μm below an epidermis phantom.**

Keywords: Visualization of blood vessels, Contrast image, Discrete Wavelet Transform, Digital Image Processing.

I. INTRODUCTION

The visualization of blood vessels is of fundamental importance for a wide variety of biomedical applications, such as in neuroscience [1]–[3], dermatology [4], [5] and ophthalmology [6], [7]. One way to analyze the dynamics of blood flow and health status of biological tissue non-invasive is through Laser Speckle Imaging (LSI). Laser Speckle is a phenomenon of random dispersion that can only be described statistically by means of a Gaussian distribution [8]. Speckle phenomenon occurs when photons from a coherent light laser interact with a rough surface (such as biological tissue) and generate scattering of photons out of the surface. If the scattered photons are acquired by CCD camera, a pattern of dark and bright points is produced, this pattern is called Raw Speckle Image (RSI) [9]. Movement of particles (such as blood cells) within the surface is seen as a blurring effect, analysis of this effect is the basis of LSI [10].

For deep blood vessels, LSI systems have some limitations due to strong scattering by static structures (such as the skull or epidermis) [8], [11]. One of the main drawbacks is related to the visualization and location of the blood vessels since the RSI images become noisier as the depth increases ($\rho > 300\mu m$) [12], however, there are some methods to deal with this drawback. Contrast image improves the visualization of RSI images by calculating the contrast using spatial, temporal and spatiotemporal algorithms [11]. The relevance to locate the blood vessels in contrast images in addition to the visualization also serves to analyze the relative blood flow that can be calculated from the contrast values [13]–[16].

In this work, we present a methodology to improve the visualization and location of blood vessels in in-vitro tests of contrast images. This methodology is based on the decomposition of wavelet coefficients and consists of (i) denoising of contrast images, (ii) calculating threshold values for a bi-level distribution and operating with mathematical morphology to binarize regions of interest (ROIs) and (iii) visualizing dynamic region using it as a mask of contrast values after noise attenuation. Experimental results show that it is possible to locate blood vessels even at 700μm depth.

II. BASIC CONCEPTS

A. Laser Speckle Imaging

When a coherent light laser (in phase) interacts with a rough surface illuminating it, the photons are scattered in different directions (changes phase) from the surface. These photons propagate through a medium (such as air) and collide with each other, causing constructive and destructive interference. If these interferences are picked up by an optical detector, scattered photons create an interference pattern. This interference pattern consists of bright and dark points also called speckles. If there is no movement of particles (such as blood cells) on the surface and the laser is stable, the interference pattern does not change over time, it is called static speckle. Otherwise, when the particles are moving on the surface, the interference pattern changes over time and is called dynamic speckle [10]. The dynamic speckle can be visualized as a blurred region in the RSI images and its analysis is the basis of LSI in biomedical applications since it can be related to the movement of the cells in the blood flow.

The development of speckle theory, the instrumentation to acquire the interference patterns and methods of reconstruction of RSI images are related to the improvement of the different ways of calculating contrast images. The most used methods in contrast image are spatial contrast (s-K), temporal contrast (t-K) and spatiotemporal contrast (st-K) which is a combination of the previous two [10]. s-K offers a higher temporal resolution at the expense of spatial resolution and vice versa for the t-K, while the advantages of both can be obtained with the st-K algorithms. A way to identify the dynamic region in an RSI image is to measure how much their values vary through a contrast measure. It is expected that, due to the blurring effect generated by the movement of the blood cells, the dynamic region has lower contrast values while the opposite occurs in the static region. Following this concept, the contrast K is defined as the ratio between standard deviation σ_s and mean intensity $\langle I \rangle$ [17]:

$$K = \frac{\sigma_s}{\langle I \rangle} \tag{1}$$

Under real conditions, contrast values follow that $0 \leq K \leq 1$ [18]. Where values close to 1 indicate that the region is high contrasted (lowly homogeneous) due a great variation of values generated by random changes associated with the static region (biological tissue) and values close to 0 indicate that the region is low contrasted (highly homogeneous) and it is associated with dynamic region (blood vessels).

B. Experimental setup

The experimental setup used in this work consists of a He-Ne Laser (632.8nm) that illuminates, in a homogeneous way, a skin phantom through of an optical diffuser (ModelED1 - C20,

Thorlabs Inc.) as shown in Fig. 1. A set of raw speckle images of the phantom surface is acquired by a CDD camera (Model-Retiga2000R, QImaging, Canada) equipped with a macro lens. The skin phantoms were fabricated with optical properties (scattering coefficient) similar to human skin, following the recipe reported in [20]. Two phantoms were used: one for epidermis and one for dermis. Different thicknesses of epidermis layer were used from $0\mu m$ to $900\mu m$.

In order to simulate the blood vessels in the dermis phantom, we use two configurations: (a) a straight glass capillary with an inner diameter of $700\mu m$ and (b) a bifurcated microchannel with an inner diameter of $300\mu m$ (thinXXS Microtechnology AG, Germany). Both were located on the dermis surface. Intralipid infusion at 3% in water was used to simulate the scattering properties of human blood and was pumped through the capillaries and a pump (Model NE-500, NewEraPumpSystemInc) controlled the blood flow. Speeds between $2mm/s$ and $20mm/s$ were considered.

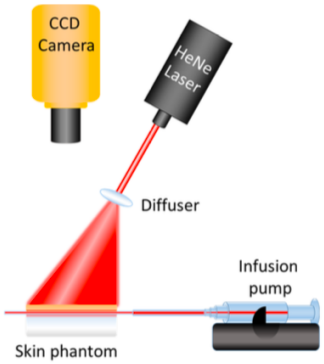

Fig. 1: Experimental setup.

C. Discrete Wavelet Transform

Wavelet Transform (WT) is an efficient technique for the local analysis of non-stationary and fast transient signals and images. WT provides multiresolution analysis with expanded windows (wavelet function), the high-frequency analysis is done using narrow windows and the low-frequency analysis is done using wide windows. WT has great advantages over other techniques of domain change (for example, Fourier domain), especially in signals and images with a wide frequency spectrum [21]. Recently, the wavelet domain has attracted interest in noise elimination (denoising) since it provides a better spatial and spectral resolution in images [22], [23].

The implementation of WT for discrete values is known as Discrete Wavelet Transform (DWT) and can be interpreted as analysis (decomposition) and synthesis (reconstruction) process for multiple levels ℓ of a discrete signal or image with frequencies between 0 and π [24]. In digital images, the analysis process of DWT separates spectral information of an image $\bar{I}(i,j)$ of size $M \times N$ into two frequency bands using high pass ($\bar{h}$) and low pass ($\bar{g}$) filters defined by a wavelet function ψ [25], [26]. After filtering goes through a process of downsampling ($\downarrow 2$) where the dimensions of the image are reduced by 2^{ℓ} (Fig. 2).

The result of the DWT analysis process are approximation and detail coefficients for the first level of decomposition ($\ell = 1$) (Fig. 3a). Approximation coefficients ($LL_{\ell=1}$) correspond to the first frequency band (0 to $\pi/2$) of low-frequency information where the maximum frequency is $\pi/2$. While, the horizontal, vertical and diagonal detail coefficients ($HH_{\ell=1}$, $HL_{\ell=1}$ and $LH_{\ell=1}$) correspond to the second frequency band ($\pi/2$ to π) of high-frequency information where the maximum frequency is π. The dimensions for any coefficient of the first level of decomposition are $M/2^{\ell=1} \times N/2^{\ell=1}$.

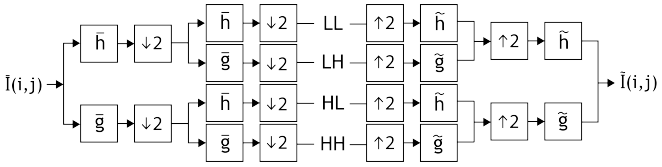

Fig. 2: DWT implementation as a filter bank for the first level of decomposition. Analysis (left) and synthesis (right) of image $\bar{I}(i,j)$ through decomposition filters ($\bar{h}$ and $\bar{g}$) and reconstruction ($\tilde{h}$ and $\tilde{g}$).

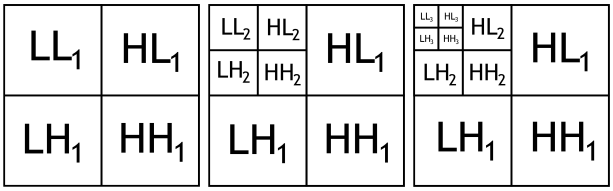

Fig. 3: Organization of the approximation (LL_{ℓ}) and detail (LH_{ℓ}, HL_{ℓ} and HH_{ℓ}) coefficients during the DWT analysis process for (a) $\ell = 1$, (b) $\ell = 2$ and (c) $\ell = 3$.

To perform a second decomposition level ($\ell = 2$), any coefficient (approximation or detail) can be analyzed, depending on the type of application. In image denoising, the analyzed coefficients are usually of approximation due to they conserve global information (such as shapes), while detail retains local information (such as noise). If the decomposition process DWT is performed in the coefficient $LL_{\ell=1}$ for $\ell = 2$, the approximation ($LL_{\ell=2}$) and detail ($HH_{\ell=2}$, $HL_{\ell=2}$ and $LH_{\ell=2}$) coefficients of dimensions $M/2^{\ell=2} \times N/2^{\ell=2}$ are obtained (Fig. 3b). The frequency band of the approximation coefficient is from 0 to $\pi/4$, while the detail coefficients is from $\pi/4$ to $\pi/2$. The synthesis process can be carried out as many times as possible under the consideration that it can be downsampled ($\downarrow 2$) after the filtering process.

The synthesis process is the inverse process of analysis. In the synthesis process given a level of decomposition $\ell \geq 1$ it is possible to reassemble the information of any coefficient (LL_{ℓ}, HL_{ℓ}, LH_{ℓ}, HH_{ℓ}) through the processes of oversampling ($\uparrow 2$) and filtering ($\tilde{g}$ and $\tilde{h}$). In image denoising the synthesis process is usually used to assemble only approximation coefficient (LL_{ℓ}) of the lowest frequency of size $M/2^{\ell} \times N/2^{\ell}$, while the detail coefficients are processed as coefficients of empty elements that only conserve the size of the coefficient. This process allows to eliminate information of the high-frecuency bands and to recover a synthesized image $\tilde{I}(i,j)$ of dimensions $M \times N$.

D. Multilevel thresholding

Thresholding is one of the most used methods in segmentation due to its easy implementation through one or more thresholds (T). Thresholding is useful to differentiate classes in a gray level image where each pixel has an intensity value $L = \{0,1,2,\ldots,255\}$ [27]. Usually, the image is divided in two or more classes depending on its intensity value (L). Equation (2) corresponds to two classes of thresholding:

$$\begin{aligned} C_1 &\longleftarrow p(i,j) \;\; if \;\; 0 \leq p < T \\ C_2 &\longleftarrow p(i,j) \;\; if \;\; T \leq p < L-1 \end{aligned} \tag{2}$$

where $p(i,j)$ is a pixel of image $I(i,j)$ of $M \times N$ dimensions, C_1 and C_2 are the classes in which the pixel $p(i,j)$ can be classified and T is the threshold value. Equation (2) can be extended for more than two classes [28]:

$$
\begin{aligned}
C_1 &\longleftarrow p(i,j) \;\; if \;\; 0 \leq p < T_1, \\
C_2 &\longleftarrow p(i,j) \;\; if \;\; T_1 \leq p < T_2, \\
C_{i+1} &\longleftarrow p(i,j) \;\; if \;\; T_i \leq p < T_{i+1}, \\
C_n &\longleftarrow p(i,j) \;\; if \;\; T_k \leq p < L-1
\end{aligned} \tag{3}
$$

where $\{T_1, T_2, \ldots, T_k\}$ represent threshold values. The thresholding drawback is to select the most appropriate threshold value T to separate classes. The Otsu method is used to calculate an automatic threshold that best separates two classes in an image. This method assumes that the image has two classes of pixels (foreground and background) following a bi-level distribution in the histogram. Otsu calculates the best threshold separating two classes, so that, if its intraclass variance is minimal the method can be extended to multi-level thresholding referred to as Multi Otsu's method [29].

E. Morphological opening

Mathematical morphology can be defined as the theory for the analysis of spatial structures but also a powerful technique for the analysis of images. The morphological operators extract a set of structures with relevant shape and size in an image I. The way to extract these structures is to compare to another set so-called elemental structuring element B, where each pixel p of the image I is analyzed through a structural element B. B is usually an odd square-shaped window of size λ denoted as $(2\lambda+1)\times(2\lambda+1)$ where λ is the scale of B [30].

The opening (γ) is an important operator used in mathematical morphology, commonly applied to binary images, and is based on the combination of the two fundamental morphological operators: erosion $\varepsilon_B(I) = \{p \mid B \subset I\}$ and dilation $\delta_B(I) = \{p \mid B \cap I \neq 0\}$. The opening γ of an image I by a structuring element B is denoted by $\gamma_B(I)$ and is defined as:

$$
\gamma_B(I) = \delta_B[\varepsilon_B(I)] \tag{4}
$$

Opening removes small objects from the foreground of an image, placing them in the background, and is used to find objects where a specific structuring element can fit being less destructive than erosion in general [31].

III. METHODOLOGY

The following methodology is based on the assumption that contrast images have two ROIs (Fig. 4a): dynamic region (blood vessel) and static region (biological tissue). The dynamic region is associated with the movement of particles and as the depth increases in the sample, the noise in the dynamic region is more intense (Fig. 4b). The noise makes difficult to calculate the threshold to segment both regions, as well as reducing the visualization and location of the blood vessel in contrast images.

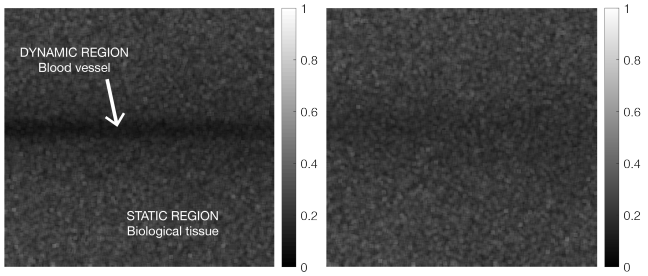

(a) (b)

Fig. 4: Contrast images (a) at $200\mu m$ (superficial blood vessel) and (b) $700\mu m$ (deep blood vessel).

In this work, we using a methodology to (i) denoising contrast images through the DWT decomposition, (ii) segmenting the ROIs by calculating threshold values to improve the location of the dynamic region with morphological operators and finally (iii) using the segmented blood vessel as a mask of contrast values to visualize the dynamic region with low noise level.

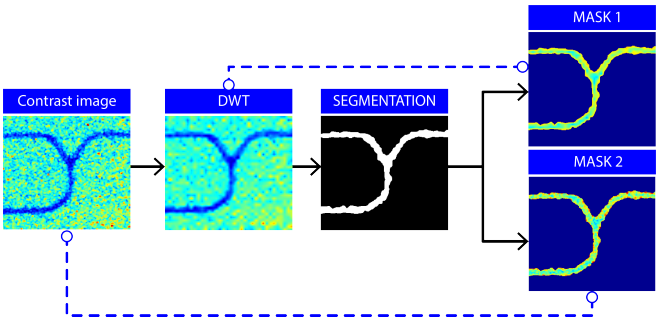

Fig. 5: Block diagram of the using methodology.

Figure 5 shows the methodology using in this work, where the input is a contrast image. DWT is the filtering process of the contrast image (synthesized image). SEGMENTATION is the thresholding and mathematical morphology of the synthesized image and finally, the output (MASK 1) is a mask with the values of the contrast image after noise attenuation, and MASK 2 is a mask with the values of contrast image. Below is a comparison between MASK 1 and MASK 2.

A. Denoising based on DWT

Consider as input a contrast image (Fig. 6a) with the following characteristics: a noisy image due to the phenomenon described in section II-B, a frequency spectrum from 0 to π and where its histogram follows a Gaussian distribution as shown in (Fig. 6c). Given the above considerations, it is difficult to establish the limits of the ROIs (static and dynamic) through the calculation of a threshold value (T). To address this limitation, the DWT analysis in contrast images is used. The objectives of analyzing contrast images through DWT are (i) reduce high-frequency noise by selectively selecting a band with the lowest frequency information that best represents the dynamic region, and (ii) obtain a bi-level histogram distribution that allows separating the ROIs facilitating the calculation of the value threshold (T).

The process of DWT analysis in contrast images is for three levels of decomposition $\ell = \{1,2,3\}$, the iterative process is performed in approximation coefficients $LL_{\ell=1}$ and $LL_{\ell=2}$. The wavelet function used was Daubechies 5 ($\psi = db_5$). The criterion is taken to select ℓ was (i) the size of the contrast image and (ii) the similarity of approximation coefficients for $\ell > 4$. On the other hand, the criterion taken to select the wavelet function is based on the results of the segmentation.

After obtaining the coefficients (LL_3 LH_3, HL_3 and HH_3) corresponding to $\ell = 3$ through the DWT analysis process, the inverse process is performed. Since the objective is to eliminate the high-frequency noise, the information of the approximation coefficient LL_3 is used as the basis of reconstruction in the DWT synthesis process, while the detail coefficients (LH_3, HL_3 and HH_3) are considered empty sets conserving their dimensions. Since when removing the information from the detail coefficients of $\ell = 3$ a new approximation coefficient LL_2 is generated without high-frequency noise. Then the same procedure is performed to generate the new approximation coefficients for $\ell = 2$ and $\ell = 1$.

The result is a synthesized image (Fig. 6b) with low-frequency information. In the distribution of the histogram (Fig. 6d) it can be seen that by eliminating the high-frequency information it is possible to identify two peaks corresponding to the ROIs separated by a valley.

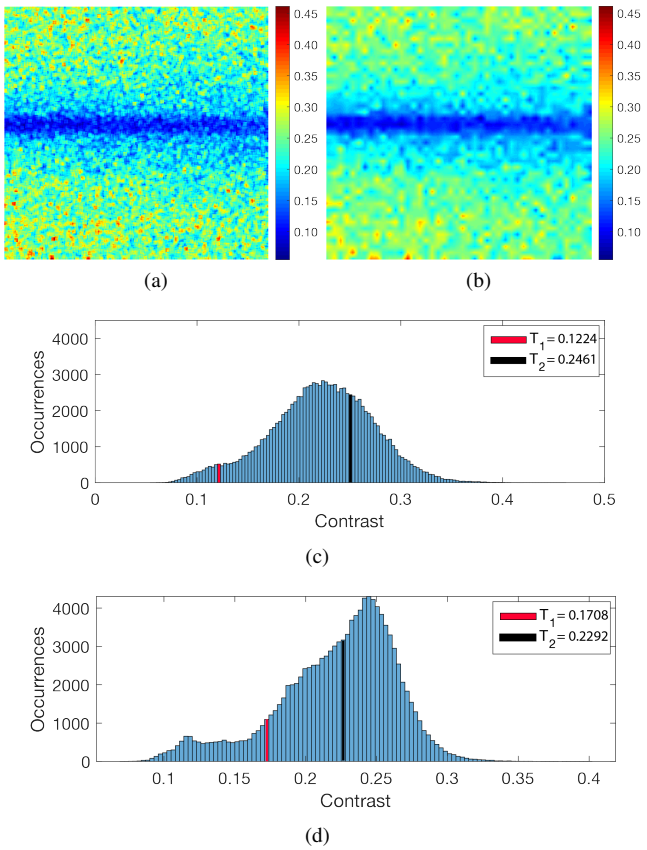

Fig. 6: Comparison between (a) contrast image and (b) synthesized image of blood vessel at $200\mu m$ depth and (c, d) their corresponding histograms.

B. Low-frequency thresholding

Let be the Fig. 6d a histogram of the synthesized image in Fig. 6b where there are two peaks separated by a valley (bi-level). The small peak represents the information of the dynamic region. The large peak corresponds to the information of the static region and the valley corresponds to the transition region between ROIs.

For segmenting of the dynamic region in the synthesized images it is required to binarize as foreground the region closest to the dynamic region and not an intermediate point between ROIs (Otsu method). Given the above, it is possible to calculate two threshold values to locate three classes (dynamic, transition and static) in the synthesized image using the segmentation method of section II-D.

In Figure 6d the first threshold ($T_1 = 0.1708$, red line) is for the region closest to the dynamic region and the second threshold ($T_2 = 0.2292$, black line) is for the region closest to the static region. From the calculation of two thresholds it is possible to establish three classes: dynamic region ($0 < C_1 < T_1$), transition region ($T_1 < C_2 < T_2$) and static region ($T_2 < C_3 < 1$). To simplify and reduce the number of classes to generate a binary image, it is proposed to join two classes in the following way:

$$I_{bin} = \begin{cases} 1, & if \quad C_1 < T_1 \\ 0, & otherwise \end{cases} \tag{5}$$

After binarizing, usually, the segmented image presents a connected region and small particles around the vessel. The binary image is operated with a morphological aperture with a circular structural element of radius $\lambda = 5$. Then, the particles that are around the blood vessel are eliminated or shrunk depending on their size. Subsequently, cleaning is performed by an area criterion, where the larger elements are maintained and the remaining small particles are eliminated. The segmented image is used as a binary marker to generate the reconstruction masks. The reconstruction mask is a way of visualizing the region corresponding to the blood vessel with an approximation to the information after noise attenuation of the contrast image. That is, the mask is reconstructed using the segmented image and the contrast values in the synthesized image.

IV. RESULTS

The set of RSI images used to test the proposed methodology consists of 30 raw speckle images for in-vitro blood vessels. The dimensions of the in-vitro images for straight vessels and bifurcated vessels are 344×329 pixels and 280×288 pixels, respectively. In the straight vessels were tested at depths of 0μm, 200μm, 400μm, 500μm, 600μm, 700μm and 900μm, while bifurcated vessels were tested at depths of 200μm, 300μm, 400μm, 500μm, 600μm, 700μm and 900μm. The RSI image packages were obtained through the experimental configuration described in section II-B. Contrast images are computed with the spatial algorithm by using an analysis window of 5×5.

Through the proposed methodology is possible to find a dynamic region (low-frequency) corresponding to the blood vessels in contrast images. This is a difficult task since the contrast images are naturally noisy but also the noise level increases with depth. Then, the results presented are focused on denoising high-frequency in contrast images, to visualize the contrast values after noise attenuation in the class corresponding to the dynamic region.

Consider, a straight blood vessel at $200\mu m$ depth (Fig. 7a), where the noise level is low and a frequency spectrum from 0 to π. In contrast image, a representation of contrast allows differentiating between ROIs. However, it is difficult to define the limits between both regions through a threshold value (Fig. 7a). By the DWT analysis of an contrast image using as basis the approximation coefficients for three levels of decomposition $\ell = \{1,2,3\}$ and a wavelet function $\psi = db_5$, we obtain the approximation (LL_ℓ) and the detail coefficients (LH_ℓ, HL_ℓ and HH_ℓ) described in Table I.

TABLE I: Bands of frequency and size of coefficients during the synthesis process.

ℓ	Approximation	Detail	Size $(M/2^\ell \times N/2^\ell)$
1	$0 - \pi/2$	$\pi/2 - \pi$	164×172
2	$0 - \pi/4$	$\pi/4 - \pi/2$	82×86
3	$0 - \pi/8$	$\pi/8 - \pi/4$	41×43

Let $LL_{\ell=3}$ be a coefficient that contains the information of lowest frequency in the band (0 to $\pi/8$) of a contrast image and it is the coefficient of interest to perform the synthesis process DWT. As described in sections II-C and III-A, it is possible to reconstruct the image without the high-frequency components during the DWT synthesis process using only the information of its coefficient. The result of the synthesis process is a synthesized image (Fig. 7b) with only low-frequency information (0 to $\pi/8$). This allows to improve the visualization of the ROIs and consequently improves the calculation of the limits of both regions through one or more thresholds.

Then, two threshold values ($T_1 = 0.1708$ and $T_2 = 0.2292$) are calculated to identify three classes (dynamic, transition and static regions) in a synthesized image as described in sections II-D and III-B. From the calculation of the thresholds values (T_1 and T_2) and the use of (5), the number of classes is reduced from three to two. These two classes are the new ROIs (dynamic and static regions) of a binary image (Fig. 7c). Then, the binary image is operated with a morphological aperture to eliminate particles that are partially outside the structure or are isolated (Fig. 7d). However, some particles isolated from the structure were not removed because

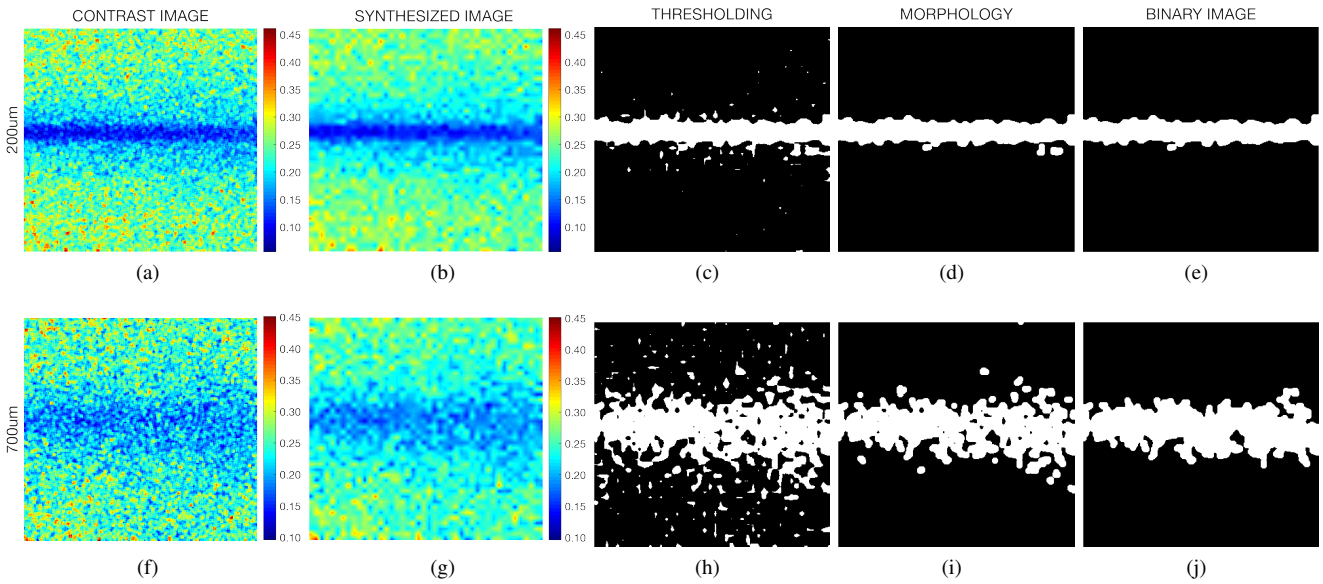

Fig. 7: Results of denoising and segmentation for (top row) 200μm depth and (down row) 700μm depth.

the size of the structural element was not sufficient for it. Then, an area criterion is applied to eliminate those isolated structures and keeping only the larger element which corresponds to the blood vessel (Fig. 7e). When the ROIs are separated into two classes, the values of the dynamic region (foreground) of a binary image are used as a mask to display the original values of an image. According to the methodology, in order to internally compare the results of the DWT synthesis process in contrast images, two masks are constructed with the values of (i) contrast image and (ii) synthesized image.

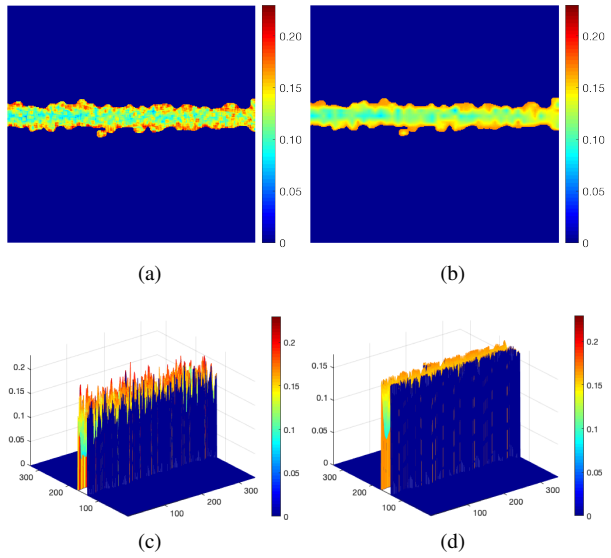

Fig. 8: Frontal and lateral view of values extracted from the contrast image (left column) and from the synthesized image (right column) by using the binary marker of Fig. 7e.

In MASK 1 (Fig. 8a, top view) constructed from the values of a contrast image is a noisy image due to its wide frequency spectrum and its contrast values. A wide frequency spectrum (0 to π) indicates that MASK 1 mixes high and low-frequency information. On the other hand, the contrast values have a random distribution and therefore, the range of values is greater as the depth increases. MASK 1 has a range of contrast values of $\Delta_{M1} = 0.1745$ where the minimum value is 0.0550 and the maximum value is 0.2296. In (Fig. 8c, lateral view) it is difficult to locate the central value in the dynamic region because it is noisy. The information of the central values is important to know the depth to which the blood vessel is located.

In MASK 2 (Fig. 8b, top view) constructed from the contrast values of a synthesized image, a homogeneous behavior on the dynamic region can be observed, this is due to the narrow range of frequencies as well as contrast values. The contrast values on MASK 2 are less noisy due to keeping the lowest frequency band (0 to $\pi/8$) and eliminating any spectrum greater than $\pi/8$ in the DWT synthesis process. On the other hand, the homogeneity of MASK 2 over the dynamic region reduces the range of values to $\Delta_{M2} = 0.0998$, where the minimum value is 0.0710 and the maximum value is 0.1708. In (Fig. 8d, lateral view) shows a dynamic region after noise attenuation, where the contrast value increases when it is closer to the edge, and the contrast values decrease when they are closer to the central region.

Now consider, a straight blood vessel at 700μm depth (Fig. 7f) where the noise level is higher. Noise reduces the visualization of ROIs and it is difficult to identify boundaries between regions. According to this limitation and following the proposed methodology the process of analysis and synthesis DWT is applied to the contrast image. The frequency spectrum is limited to keep the low-frequency information in a band from 0 to $\pi/8$, and eliminating the high-frequency information greater than $\pi/8$. Although the synthesized image is noisy, it is possible to perform the threshold calculation to separate the ROIs. The resulting binary marker (Fig. 7j) was used for extracting MASK 1 and MASK 2 from the contrast and synthesized images as shown in Fig. 9. The comparison of the results for both masks is presented in Fig. 9. The mask extracted from the contrast image (Fig. 9a and 9c) is noisier because the depth and it has a wide spectrum of frequencies (0 to π). On the other hand, the mask extracted from the synthesized image (Fig. 9b and 9d), has contrast values more homogeneous in the dynamic region because only the frequencies of the band are preserved (0 to $\pi/8$).

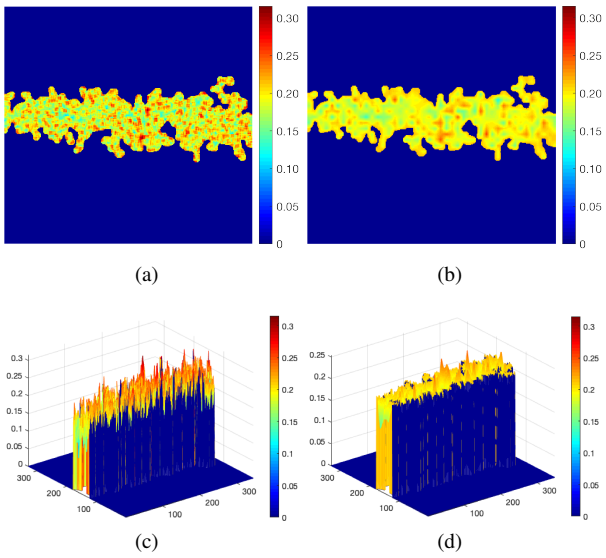

Fig. 9: Frontal and lateral view of values extracted from the contrast image (left column) and from the synthesized image (right column) by using the binary marker of Fig. 7j.

V. CONCLUSIONS

The visualization of blood vessels is an important task for diverse applications of monitoring in biomedical. The biggest drawback in the contrast images is the noise level that increases with depth, reducing the visualization of the blood vessels. In this work, we presented a methodology for high-frequency noise denoising in contrast images using DWT analysis and synthesis. In addition, the segmentation of ROIs is performed by calculating the threshold to separate the dynamic and static region, as well as the binarization for two classes and the operation with mathematical morphology. Finally, the masks are compared with the values of contrast before and after noise attenuation, where it is demonstrated that the use of the DWT is useful to reduce the noise and improve the visualization of the blood vessel even in deep blood vessels.

REFERENCES

[1] G. A. Armitage, K. G. Todd, A. Shuaib, and I. R. Winship, "Laser speckle contrast imaging of collateral blood flow during acute ischemic stroke". *Journal of Cerebral Blood Flow & Metabolism*, vol. 30, no. 8, pp. 1432–1436, Aug. 2010.

[2] Z. Wang, W. Luo, P. Li, J. Qiu, and Q. Luo, "Acute hyperglycemia compromises cerebral blood flow following cortical spreading depression in rats monitored by laser speckle imaging". *Journal of Biomedical Optics*, vol. 13, no. 6, pp. 64023–64026, 2008.

[3] P. Li, S. Ni, L. Zhang, S. Zeng, and Q. Luo, "Imaging cerebral blood flow through the intact rat skull with temporal laser speckle imaging". *Optics Letters*, vol. 31, issue 12, pp. 1824-1826, 2006.

[4] B. Choi, N. M. Kang, and J. S. Nelson, "Laser speckle imaging for monitoring blood flow dynamics in the in vivo rodent dorsal skin fold model". *Microvascular Research*, vol. 68, pp. 143-146, 2004.

[5] B. Choi, J. C. Ramirez-San-Juan, J., Lotfi, and J. S. Nelson, "Linear response range characterization and in vivo application of laser speckle imaging of blood flow dynamics". *Journal of biomedical optics*, vol. 11(4), pp. 041129, 2006.

[6] A. Ponticorvo, D. Cardenas, A. K. Dunn, D. Tso, and T. Q. Duong, "Laser speckle contrast imaging of blood flow in rat retinas using an endoscope". *Journal of biomedical optics*, vol. 18, no. 9, p. 90501, 2013.

[7] A. I. Srienc, Z. L. Kurth-Nelson, and E. A. Newman, "Imaging retinal blood flow with laser speckle flowmetry". *Frontiers in Neuroenergetics*, vol. 2, pp. 2-128, 2010.

[8] D. Briers, D. Duncan, S. Kirkpatrick, M. Larsson, T. Stromberg, and O. Thompson, "Laser speckle contrast imaging: Theoretical and practical limitations". *Journal of biomedical optics*, vol. 18, no. 6, pp. 1–9, 2013.

[9] Y. A. Aizu and T. Asakura, "Bio-speckle phenomena and their application to the evaluation of blood flow". *Optics & Laser Technology*, vol 23, no. 4, pp. 205–219, 1991.

[10] M. Draijer, E. Hondebrink, T. van Leeuwen, and W. Steenbergen. "Review of laser speckle contrast techniques for visualizing tissue perfusion". *Lasers in medical science*, vol. 24, no. 4, pp. 639–651, 2009.

[11] P. G. Vaz, A. Humeau-Heurtier, E. Figueiras, C. Correia, and J. Cardoso. "Laser speckle imaging to monitor microvascular". *IEEE reviews in biomedical engineering*, vol. 9, pp. 106–120, 2016.

[12] J. O'Doherty, P. McNamara, N. T. Clancy, J. G. Enfield, and M. J. Leahy. "Comparison of instruments for investigation of microcirculatory blood flow and red blood cell concentration". *Journal of biomedical optics*, vol. 14, no. 3, pp. 034025, 2009.

[13] H. Cheng, Q. Luo, Q. Liu, Q. Lu, H. Gong, and S. Zeng, "Laser speckle imaging of blood flow in microcirculation". *Physics in Medicine & Biology,*, vol. 49, no. 7, pp. 1347, 2004.

[14] M. S. Smith, E. F. Packulak, and M. G. Sowa, "Development of a laser speckle imaging system for measuring relative blood flow velocity". *International Society for Optics and Photonics*, vol. 6343, pp. 634304, 2006.

[15] E. Morales-Vargas, J. Sosa-Martinez, H. Peregrina-Barreto, J. Rangel-Magdaleno and J. C. Ramirez-San-Juan, "A morphological approach for locating blood vessels in laser contrast speckle imaging". *IEEE International Instrumentation and Measurement Technology Conference (I2MTC)* pp. 1-6, May, 2018.

[16] H. Peregrina-Barreto, E. Perez-Corona, J. Rangel-Magdaleno, R. Ramos-Garcia, R. Chiu and J. C. Ramirez-San-Juan, "Use of kurtosis for locating deep blood vessels in raw speckle imaging using a homogeneity representation". *Journal of biomedical optics*, vol. 22, no. 6, pp. 066004, 2017.

[17] D. D. Duncan and S. J. Kirkpatrick, "Can laser speckle flowmetry be made a quantitative tool?". *Journal of the Optical Society of America*, vol. 25, no. 8, pp. 2088–2094, Aug. 2008.

[18] J. D. Briers and A.F. Fercher, "Retinal blood-flow visualization by means of laser speckle photography". *Investigative ophthalmology & visual science*, vol. 22, no. 2, pp. 255–259, 1982.

[19] A. K. Dunn, "Laser speckle contrast imaging of cerebral blood flow". *Annals of biomedical engineering*, vol. 40, no. 2, pp. 367–377, 2012.

[20] R. B. Saager, C. Kondru, K. Au, K. Sry, F. Ayers, and A. J. Durkin, "Multilayer silicone phantoms for the evaluation of quantitative optical techniques in skin imaging". *International Society for Optics and Photonics*, vol. 7567, pp. 756-706, 2010.

[21] Y. Wang, W. Wu, Q. Zhu, and G. Shen, "Discrete Wavelet Transfom for Nonstationary Signal Processing". *Discrete Wavelet Transforms-Theory and Applications*, InTech, 2011.

[22] P. C. V. Amulya, and S.V. Lakshmi. "Image Denoising with Wavelet Based Thresholding". *IOSR Journal*. vol. 18, pp. 01-04, 2016.

[23] S. G. Chang, B. Yu, and M. Vetterli, "Adaptive wavelet thresholding for image denoising and compression". *IEEE transactions on image processing*,vol. 9, no. 9, pp. 1532-1546, 2000.

[24] S. G. Mallat, "A theory for multiresolution signal decomposition: the wavelet representation". *IEEE transactions on pattern analysis and machine intelligence*, vol. 11, no. 7, pp. 674-693, 1989.

[25] S. G. Mallat, "A wavelet tour of signal processing". *Elsevier*, 1999.

[26] I. Daubechies, "Ten lectures on wavelets". Vol. 61 *Siam*, 1992.

[27] S. Kotte, P. R. Kumar, and S. K. Injeti, "An efficient approach for optimal multilevel thresholding selection for gray scale images based on improved differential search algorithm". *Ain Shams Engineering Journal* , 2016.

[28] P. S. Liao, T. S. Chen and P. C. Chung, "A fast algorithm for multilevel thresholding". *Journal of Information Science and Engineering*. vol. 17, no. 5 pp.713-727, 2001.

[29] N. Otsu, "A threshold selection method from gray-level histograms". *EEE transactions on systems, man, and cybernetics*, vol. 9, no. 1, pp. 62-66, 1979.

[30] P. Soille, "Morphological image analysis: principles and applications". *Springer Science & Business Media*, 2013.

[31] E. R. Davies, "Computer and machine vision: theory, algorithms, practicalities". *Academic Press*, 2012.